REPORT

QUANTUM SIMULATION

Many-body–localized discrete time crystal with a programmable spin-based quantum simulator

J. Randall[1,2]†, C. E. Bradley[1,2]†, F. V. van der Gronden[1,2], A. Galicia[1,2], M. H. Abobeih[1,2], M. Markham[3], D. J. Twitchen[3], F. Machado[4,5], N. Y. Yao[4,5], T. H. Taminiau[1,2]*

The discrete time crystal (DTC) is a nonequilibrium phase of matter that spontaneously breaks time-translation symmetry. Disorder-induced many-body localization can stabilize the DTC phase by breaking ergodicity and preventing thermalization. Here, we observe the hallmark signatures of the many-body–localized DTC using a quantum simulation platform based on individually controllable carbon-13 nuclear spins in diamond. We demonstrate long-lived period-doubled oscillations and confirm that they are robust for generic initial states, thus showing the characteristic time-crystalline order across the many-body spectrum. Our results are consistent with the realization of an out-of-equilibrium Floquet phase of matter and introduce a programmable quantum simulator based on solid-state spins for exploring many-body physics.

A time crystal spontaneously breaks time-translation symmetry (*1–3*). Understanding the consequences and limitations of this idea has motivated intense exploration across a multitude of physical settings (*4–8*). A particularly fruitful case has been that of isolated periodically driven (Floquet) quantum systems, in which the stability of time crystals is connected to fundamental questions in nonequilibrium statistical mechanics (*4*, *5*, *9–11*).

In a Floquet system, the spontaneous breaking of the time-translation symmetry associated with the periodic drive results in a discrete time crystal (DTC) (*9–11*). The DTC is a new phase of matter that locks onto a period that is a multiple of that of the drive and is stable against perturbations. Experiments have revealed signatures of discrete time-crystalline behavior in a range of systems including trapped ions (*12*, *13*), spin ensembles (*14–17*), ultracold atoms (*18*, *19*), and superconducting qubits (*20*).

A key challenge is that the stability of the DTC, as well as any type of order in a Floquet many-body system, requires a mechanism to avoid thermalization and heating from the periodic drive. Although there exist a number of strategies for exponentially delaying thermalization (*7*, *13*, *21–23*), the only known mechanism for breaking ergodicity in a generic interacting system is disorder-induced many-body localization (MBL). Specifically in this context, DTC order is present across the full eigenspectrum of the Floquet system, translating into time-crystalline dynamics for generic initial states (*4*, *5*, *9–11*, *24*, *25*). The demonstration of such robust DTC order has remained an outstanding challenge (*4*, *26*).

Here, we present an observation of the hallmark signatures of the many-body–localized DTC phase. We develop a quantum simulator based on individually controllable and detectable ^{13}C nuclear spins in diamond, which can be used to realize a range of many-body Hamiltonians with tunable parameters and dimensionalities. We implement a Floquet sequence in a one-dimensional (1D) chain of $L = 9$ spins and observe the characteristic period doubling associated with the DTC. By combining the ability to prepare arbitrary initial states with site-resolved measurements, we observe the DTC response for a variety of initial states up to $N = 800$ Floquet cycles. This robustness for generic initial states provides a key signature to distinguish the many-body–localized DTC phase from prethermal responses, which only show a long-lived response for particular states (*13*, *21*, *22*, *26*).

Our experiments are performed on a system of ^{13}C nuclear spins in diamond close to a nitrogen-vacancy (NV) center at 4 K (Fig. 1A). The nuclear spins are well-isolated qubits with coherence times up to tens of seconds (*27*, *28*). They are coupled via dipole-dipole interactions and are accessed through the optically addressable NV electronic spin (*28*, *29*). With the electronic spin in the $m_s = -1$ state, the electron-nuclear hyperfine interaction induces a frequency shift h_j for each nuclear spin, which—combined with an applied magnetic field B_z in the z direction—reduces the dipolar interactions to Ising form (*27*). We additionally apply a radio-frequency (rf) driving field to implement nuclear-spin rotations. The nuclear-spin Hamiltonian is then given by $H = H_{\rm int} + H_{\rm rf}$, where $H_{\rm int}$ and $H_{\rm rf}$ describe the interaction and rf driving terms respectively:

$$\begin{aligned} H_{\rm int} &= \sum_j (B + h_j)\sigma_j^z + \sum_{j<k} J_{jk}\sigma_j^z\sigma_k^z \\ H_{rf} &= \sum_j \Omega(t)\sigma_j^x \end{aligned} \quad (1)$$

Here, σ_j^β ($\beta = x, y, z$) are the Pauli matrices for spin j, $B = \gamma_c B_z/2$ is the magnetic field splitting, γ_c is the ^{13}C gyromagnetic ratio, J_{jk} is the zz component of the dipole-dipole interaction between spins j and k, and $\Omega(t)$ is the applied time-dependent rf field, and we set $\hbar = 1$. The system has previously been characterized in detail (*27*, *29*); for 27 ^{13}C spins, the hyperfine shifts h_j, the spatial coordinates, and the 351 interaction terms J_{jk} are known.

To investigate the DTC phase, we apply a Floquet unitary consisting of free evolution $U_{\rm int}(\tau) = \exp(-iH_{\rm int}\tau)$, interleaved with global spin rotations $U_x(\theta) = \exp\left(-i\theta\sum_j^L \sigma_j^x/2\right)$. To realize the global rotations, we develop multifrequency rf pulses that simultaneously rotate a chosen subset of spins ($H_{\rm rf}$ in Eq. 1) (*27*). We symmetrize the Floquet unitary such that $U_{\rm F} = U_{\rm int}(\tau)\cdot U_x(\theta)\cdot U_{\rm int}(\tau)$, and apply N cycles of this basic sequence (Fig. 1B). For $\theta \sim \pi$, this decouples the targeted spins from their environment while preserving the internal interactions (*27*).

To stabilize MBL, the Floquet sequence $[U_{\rm F}]^N$ should satisfy two requirements. First, the system should be low-dimensional and short-range interacting (*26*, *30–33*). This requirement is not naturally met in a coupled 3D spin system (Fig. 1A). To resolve this discrepancy, we program an effective 1D spin chain using a subset of nine spins [Fig. 1, A, C, and D (*27*)]. Second, because the periodic rotations approximately cancel the on-site disorder terms h_j, the system must exhibit Ising-even disorder to stabilize MBL in the Floquet setting (*4*, *11*, *26*). This is naturally realized in our system because the Ising couplings, J_{jk}, inherit the positional disorder of the nuclear spins. The disorder in the magnitude of the nearest-neighbor couplings is distributed over a range $W \sim 10$ Hz. The ratio of disorder to average nearest-neighbor coupling is therefore $W/J_0 \sim 1.5$, comparable with previous theoretical studies of MBL DTCs (*4*, *9*, *26*).

To reveal the signature spatiotemporal order of the DTC phase, one must prepare a variety of initial states and perform site-resolved measurements (*9*, *26*). We use a combination of new and existing methods to realize the required initialization, single-spin control, and individual single-shot measurement for all spins in the chain (Fig. 1B).

[1]QuTech, Delft University of Technology, PO Box 5046, 2600 GA Delft, Netherlands. [2]Kavli Institute of Nanoscience Delft, Delft University of Technology, P.O. Box 5046, 2600 GA Delft, Netherlands. [3]Element Six Innovation, Fermi Avenue, Harwell Oxford, Didcot, Oxfordshire OX11 0QR, UK. [4]Department of Physics, University of California, Berkeley, CA 94720, USA. [5]Materials Sciences Division, Lawrence Berkeley National Laboratory, Berkeley, CA 94720, USA.
***Corresponding author. Email: t.h.taminiau@tudelft.nl**
†These authors contributed equally to this work.

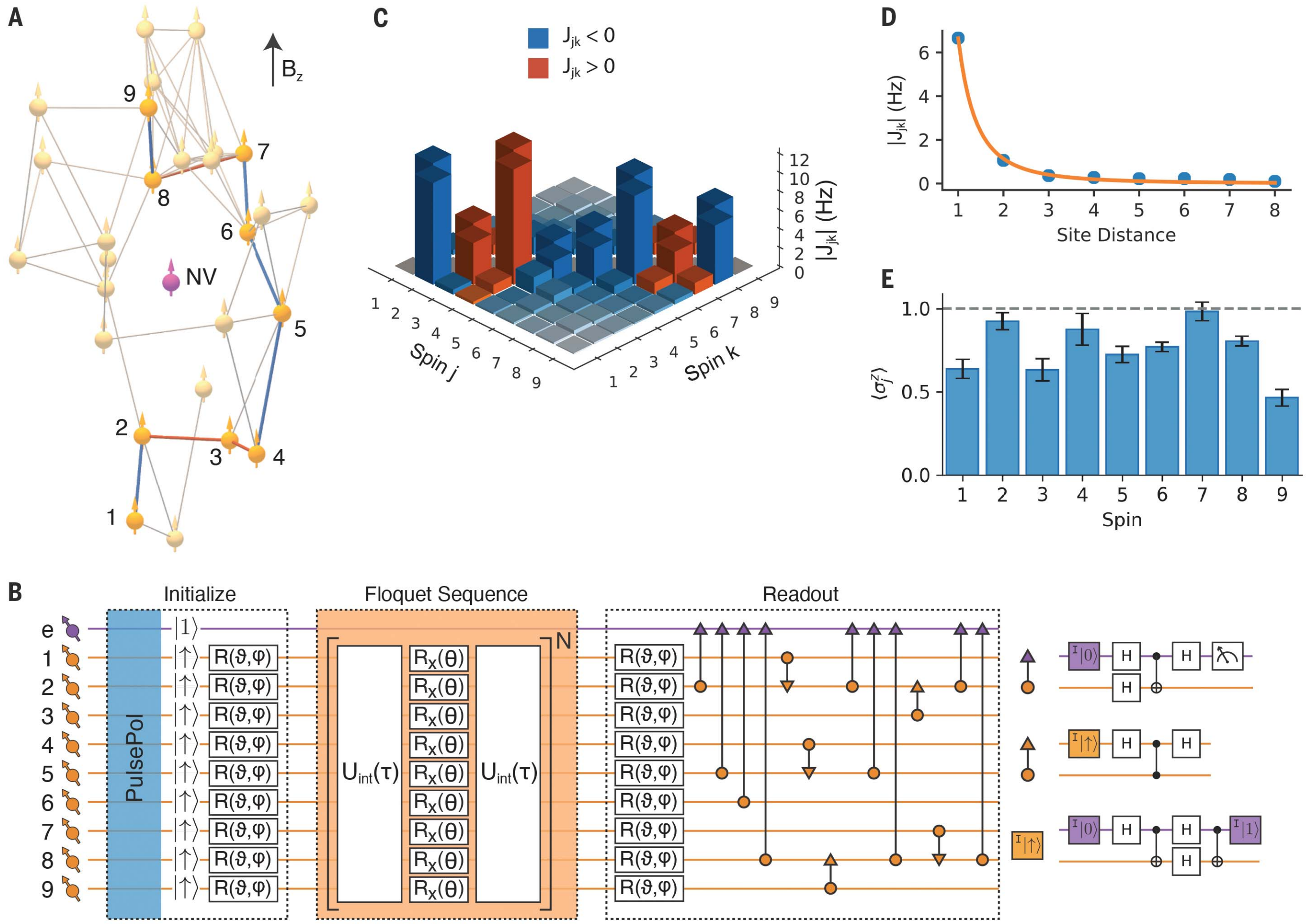

Fig. 1. Programmable spin-based quantum simulator. (**A**) We program an effective 1D chain of nine spins in an interacting cluster of 27 ^{13}C nuclear spins (orange) close to a single NV center. Connections indicate nuclear-nuclear couplings $|J_{jk}| > 1.5$ Hz, and blue (red) lines represent negative (positive) nearest-neighbor couplings within the chain (*29*). Magnetic field: $B_z \sim 403$ G. (**B**) Experimental sequence: The spins are initialized by applying the PulsePol sequence (*34*), followed by rotations of the form $R(\vartheta, \varphi) = \exp\left[-i\frac{\vartheta}{2}(\sin(\varphi)\sigma^x + \cos(\varphi)\sigma^y)\right]$. After evolution under N cycles of the Floquet unitary $U_F = U_{\text{int}}(\tau) \cdot U_x(\theta) \cdot U_{\text{int}}(\tau)$, the spins are sequentially read out through the NV electronic spin using electron-nuclear and nuclear-nuclear two-qubit gates (see text). Colored boxes with "I" denote re-initialization into the given state. (**C**) Coupling matrix for the nine-spin chain. (**D**) Average coupling magnitude as a function of site distance across the chain. Orange line: least-squares fit to a power-law function $J_0/|j-k|^\alpha$, giving $J_0 = 6.7(1)$ Hz and $\alpha = 2.5(1)$, confirming that the chain maps to an effective 1D system. (**E**) Measured expectation values $\langle\sigma_j^z\rangle$ after initializing the state $|{\uparrow\uparrow\uparrow\uparrow\uparrow\uparrow\uparrow\uparrow\uparrow}\rangle$. The data are corrected for measurement errors (*27*).

First, we initialize the spins through a recently introduced dynamic nuclear polarization sequence called PulsePol (*34*). This sequence polarizes nuclear spins in the vicinity of the NV center and prepares the 1D chain in the state $|{\uparrow\uparrow\uparrow\uparrow\uparrow\uparrow\uparrow\uparrow\uparrow}\rangle$. We analyze and optimize the polarization transfer in the supplementary materials (*27*). Subsequently, each spin can be independently rotated to an arbitrary state by selective rf pulses (*27*).

Second, after Floquet evolution, we read out the spins by sequentially mapping their $\langle\sigma_j^z\rangle$ expectation values to the NV electronic spin (*27*) and measuring the electronic-spin state by resonant optical excitation (*28*). Spins j = 2, 5, 6, 8 can be directly accessed using previously developed electron-nuclear two-qubit gates (*28*). To access the other spins (j = 1, 3, 4, 7, 9), which couple weakly to the NV, we develop a protocol based on nuclear-nuclear two-qubit gates through spin-echo double resonance [details and characterization are given in the supplementary materials (*27*)]. We use these gates to map the spin states to other, directly accessible spins in the chain. Figure 1E shows the measured $\langle\sigma_j^z\rangle$ expectation values after preparing the state $|{\uparrow\uparrow\uparrow\uparrow\uparrow\uparrow\uparrow\uparrow\uparrow}\rangle$.

We verify that we can isolate the dynamics of a subset of spins by studying the first four spins of the nine-spin chain (Fig. 2A). We prepare the superposition state $|{++++}\rangle$, where $|+\rangle = (|{\uparrow}\rangle + |{\downarrow}\rangle)/\sqrt{2}$, and apply $[U_F]^N$ with $\theta = \pi$. We first verify that the state is preserved when each spin is individually decoupled to remove interactions (Fig. 2B) (*27*). By contrast, with internal interactions, the four spins entangle and undergo complex dynamics. The measured evolution matches a numerical simulation containing only the four spins, indicating that the system is strongly interacting and protected from external decoherence.

With this capability confirmed, we turn to the nine-spin chain and the DTC phase. The expectation for the DTC phase is a long-lived period-doubled response that is stabilized against perturbations of U_F through many-body interactions. To illustrate this, we set $\theta = 0.95\pi$, a perturbation from the ideal value of π, and tune the system through the DTC phase transition by changing τ, which effectively sets the interaction strength (Fig. 3, A to C).

We first investigate the state $|\uparrow\uparrow\uparrow\uparrow\uparrow\uparrow\uparrow\uparrow\uparrow\rangle$ and consider the averaged two-point correlation function $\bar{\chi} = \frac{1}{L}\sum_{j=1}^{L}\langle\sigma_j^z(N)\rangle \mathrm{sgn}[\langle\sigma_j^z(0)\rangle]$, where $\langle\sigma_j^z(N)\rangle$ is the expectation value at Floquet cycle N for spin j. Without interactions, the deliberate under-rotations ($\theta < \pi$), in combination with naturally present noise in the applied control fields, lead to a rapid decay (Fig. 3, B and C). By introducing moderate interactions ($\tau = 1.55$ ms), the system is on the edge of the phase transition, and the interactions begin to stabilize the subharmonic response (Fig. 3, B to D). Finally, for strong interactions ($\tau = 5$ ms), the subharmonic response is stabilized despite the perturbations of θ (Fig. 3, B, C, and E). The individual spin measurements confirm that the spins are synchronized, and the signature long-lived spatiotemporal response is observed (Fig. 3E).

To rule out trivial noninteracting explanations, we prepare the superposition state $[\cos(\pi/8)|\uparrow\rangle + \sin(\pi/8)|\downarrow\rangle]^{\otimes 9}$ and perform full single-qubit tomography for each spin for different values of N (*9*). The two-point correlation $\bar{\chi}$ shows a persistent subharmonic response similar to that of the initial state $|\uparrow\uparrow\uparrow\uparrow\uparrow\uparrow\uparrow\uparrow\uparrow\rangle$ (Fig. 3F). By contrast, the coherence $\bar{C} = \frac{1}{L}\sum_{j=1}^{L}\sqrt{\langle\sigma_j^x\rangle^2 + \langle\sigma_j^y\rangle^2}$ shows a quick decay on a time scale of ~10 Floquet cycles, indicating rapid local dephasing due to internal many-body interactions that generate entanglement across the system (Fig. 3G).

Although the results shown in Fig. 3 are consistent with a DTC, these measurements alone do not distinguish the many-body–localized DTC phase from prethermal responses (*4*, *13*, *26*). In particular, the hallmark of the MBL DTC phase is robust time-crystalline order for generic initial states. Conversely, prethermal responses only exhibit long-lived oscillations for a particular range of initial states (*21*, *26*).

We study a range of generic initial states of the form $\otimes_j^L |m_j\rangle$, $m_j \in \{\uparrow, \downarrow\}$, including the

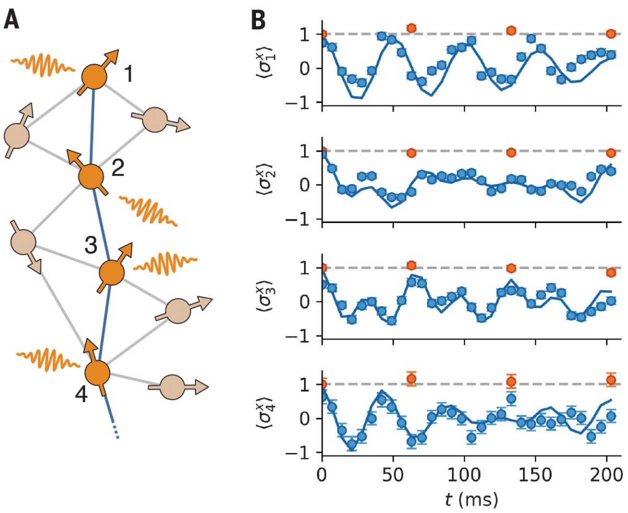

Fig. 2. Isolating spin chains. (**A**) We test the programming of interacting spin chains for the first four spins of the nine-spin chain (Fig. 1, A, C, and D). For $\theta \sim \pi$, the Floquet sequence $[U_F]^N$ decouples the spin chain from its environment but preserves the internal interactions. (**B**) Measured expectation values $\langle\sigma_j^x\rangle$ after initializing the state $|{+}{+}{+}{+}\rangle$ and applying $[U_F]^N$ with $\theta = \pi$. Here $t = 2\tau N$ is varied by fixing $\tau = 3.5$ ms and varying N. The blue (orange) points show the evolution with (without) spin-spin interactions (*27*). Blue lines: numerical simulations of only the four-spin system (*27*). Measurements in this figure and hereafter are corrected for state preparation and measurement errors.

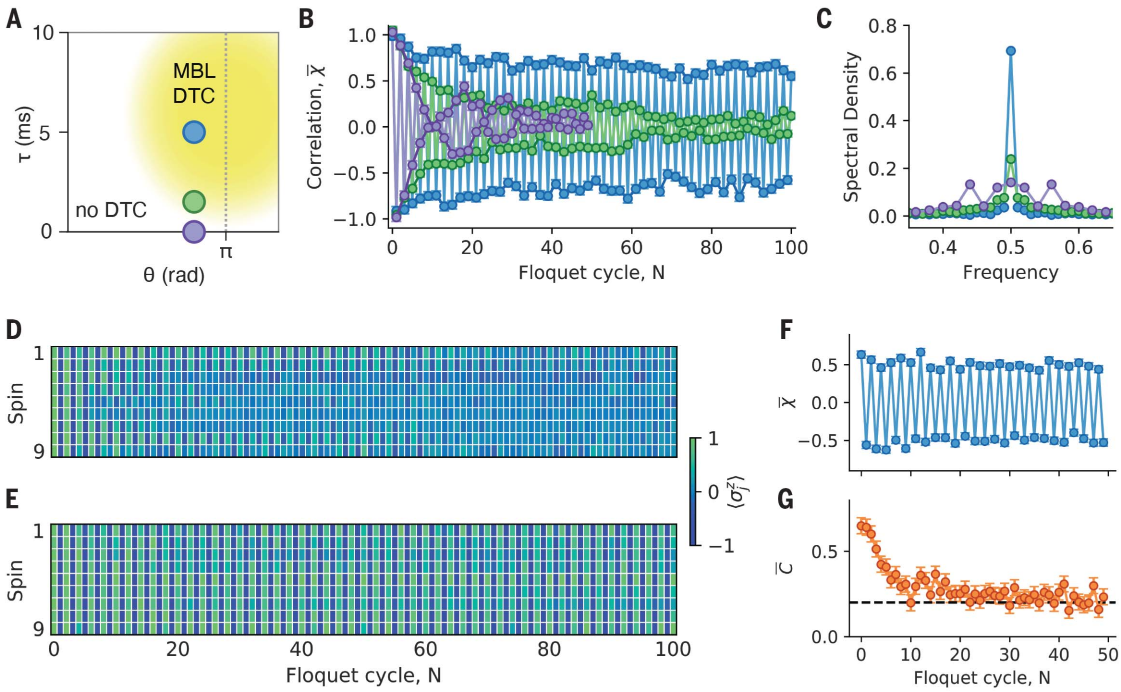

Fig. 3. Discrete time crystal in the nine-spin chain. (**A**) Sketch of the phase diagram as a function of τ and θ when applying the Floquet sequence $[U_F]^N$ (Fig. 1B) (*4*). The yellow region indicates the many-body–localized DTC phase. The colored points mark three combinations of $\{\theta, \tau\}$ that illustrate the DTC phase transition. Additional data for other values are given in the supplementary materials (*27*). (**B**) Averaged two-point correlation $\bar{\chi}$ as a function of the number of Floquet cycles N for $\theta = 0.95\pi$ and initial state $|\uparrow\uparrow\uparrow\uparrow\uparrow\uparrow\uparrow\uparrow\uparrow\rangle$. Without interactions [purple (*27*)], $\bar{\chi}$ decays quickly. With small interactions ($\tau = 1.55$ ms, green), the system is on the edge of the transition to the DTC phase. With strong interactions ($\tau = 5$ ms, blue), the subharmonic response is stable and persists over all 100 Floquet cycles. (**C**) The corresponding Fourier transforms show a sharp peak at $f = 0.5$ emerging as the system enters the DTC phase. (**D** and **E**) Individual spin expectation values $\langle\sigma_j^z\rangle$ for interaction times $\tau = 1.55$ ms (D) and $\tau = 5$ ms (E). (**F** and **G**) Averaged two-point correlation $\bar{\chi}$ (F) and coherence $\bar{C}$ (G) after preparing the superposition state $[\cos(\pi/8)|\uparrow\rangle + \sin(\pi/8)|\downarrow\rangle]^{\otimes 9}$ and applying $[U_F]^N$ with $\tau = 5$ ms. The subharmonic response in $\bar{\chi}$ is preserved, whereas $\bar{C}$ quickly decays because of interaction-induced local dephasing. The dashed line in (G) indicates a reference value for $\bar{C}$ measured after preparing the state $|\uparrow\rangle^{\otimes 9}$ (*27*).

Néel state $|\uparrow\downarrow\uparrow\downarrow\uparrow\downarrow\uparrow\downarrow\uparrow\rangle$ (Fig. 4A) and nine additional random states (Fig. 4, B and C) . To illustrate that a variety of states are considered, we evaluate their energy density $\mathcal{E} = \langle H_{\text{eff}}\rangle / J_0 L$, where J_0 is the average nearest-neighbor coupling strength (Fig. 1D) and H_{eff} is the leading order term in the Floquet-Magnus expansion of U_{F} (*27*). The selected initial states extend across the energy spectrum (Fig. 4D).

The response up to $N = 800$ shows a stable period-doubled signal for all states, consistent with a DTC stabilized by MBL (Fig. 4, A and B). The $1/e$ decay value averaged over the states is $N_{1/e} = 463(36)$ Floquet cycles—corresponding to a time of ~4.6 s (Fig. 4B), and little dependence on the state is observed (Fig. 4C). By contrast, numerical calculations for a nine-spin chain with the same average couplings, but without disorder so that there is no MBL, show a strongly state-dependent response (*27*). Some initial states show a rapid decay, falling to $1/e$ within ~30 Floquet cycles and crossing through $\bar{\chi} = 0$ within 300 cycles, showing that such a prethermal response would be well distinguished within the experimental lifetime.

Although the DTC phase in an ideal system is predicted to persist to arbitrary times, any experimental implementation inevitably decays because of finite-size effects or environmental decoherence. Numerical calculations for the spin chain without decoherence yield a long-lived response up to ~10^6 Floquet cycles, as well as an exponential growth of the DTC lifetime with system size (*27*). This result shows that the chain is sufficiently large to display the hallmark divergence of MBL (*9*) and that its finite size does not limit the observed DTC lifetime. A characterization of the decoherence [$T_2 > 4800(900)$ periods] and relaxation (T_1, none observed) times for the spins shows that these are negligible over the time scale of the experiments (*27*). Therefore, the observed decay likely originates from residual interactions with the spin environment owing to imperfect decoupling under the Floquet sequence with $\theta \neq \pi$ (*27*). Such decoherence might be mitigated in the future with improved decoupling sequences.

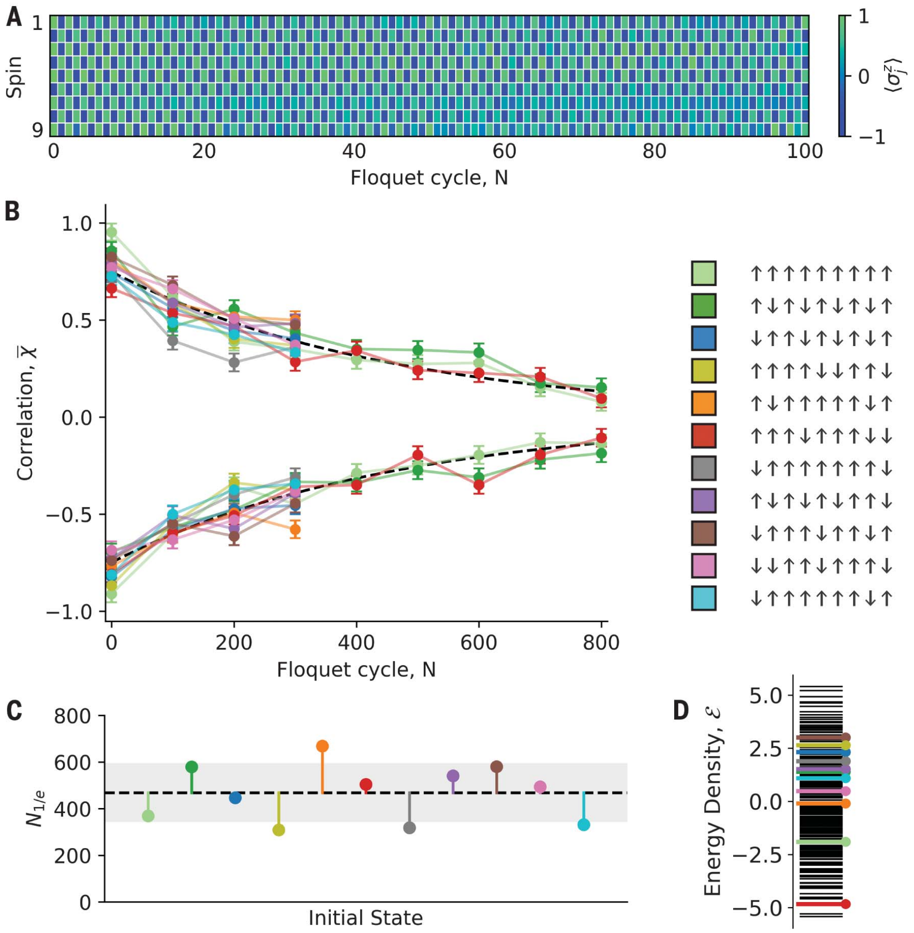

Fig. 4. Observation of the DTC response for generic initial states. (**A**) Individual spin expectation values $\langle\sigma_j^z\rangle$ as a function of N after initializing the spins in the Néel state $|\uparrow\downarrow\uparrow\downarrow\uparrow\downarrow\uparrow\downarrow\uparrow\rangle$ and applying $[U_{\text{F}}]^N$ for $\theta = 0.95\pi$ and $\tau = 5$ ms. (**B**) Average correlation for even (upper curve) and odd (lower curve) N for nine randomly chosen initial states, plus the polarized state and the Néel state (indicated in the legend) with $\theta = 0.95\pi$ and $\tau = 5$ ms. Each data point is the average over even/odd integers in the range N to $N + 10$. Three of the states are measured up to $N = 800$, the others to $N = 300$. The dashed black line is a fit of $|\bar{\chi}|$, averaged over all states using a phenomenological function $f(N) = Ae^{-N/N_{1/e}}$, giving $A = 0.75(2)$ and $N_{1/e} = 463(36)$. (**C**) $N_{1/e}$ for each initial state, extracted from a fit to $f(N)$ for the data in (B). The gray shaded region indicates the measurement uncertainty ($\pm 2\sigma$ around the mean) obtained through a Monte Carlo sampling of the fitting procedure (*27*). (**D**) Calculated energy density $\mathcal{E}$ for all possible states of the form $\otimes_j^L |m_j\rangle$, $m_j \in \{\uparrow, \downarrow\}$ (black lines). Colored lines: states indicated in the legend shown in (B).

In conclusion, we present an observation of the hallmark signatures of the many-body–localized DTC phase. Compared with previous experiments, the observed time-crystalline response is stable for generic initial states, demonstrating robust DTC order across the many-body spectrum. This result highlights the importance of both many-body interactions and disorder for stabilizing MBL-DTC order. The developed methods also provide new opportunities to investigate other Floquet phases of matter, including topologically protected phases (*4*), and time-crystalline order in a variety of settings complementary to MBL, such as open systems where the interplay between dissipation and interactions leads to distinct DTC phenomena (*6*, *7*, *35*).

From a broader perspective, this work introduces a quantum simulator based on individually controllable solid-state spins that is naturally suited to studying many-body dynamics. By connecting different subsets of spins, larger one-dimensional chains and two- and three-dimensional systems can be realized (*36*, *37*). The combination of complete programmability through universal individual control, excellent coherence, and site-selective measurement enables the realization of a wide variety of many-body Hamiltonians. Future scalability beyond tens of spins might be achieved by exploiting spins external to the diamond (*38*, *39*), by linking multiple electronic-spin defects through dipolar coupling (*40*), by photonic remote entanglement (*41*), or by combinations of these methods.

Note added in proof: While this manuscript was undergoing peer review, a related preprint appeared that reports the observation of an MBL DTC using superconducting qubits (*42*).

REFERENCES AND NOTES

1. F. Wilczek, *Phys. Rev. Lett.* **109**, 160401 (2012).
2. A. Shapere, F. Wilczek, *Phys. Rev. Lett.* **109**, 160402 (2012).
3. H. Watanabe, M. Oshikawa, *Phys. Rev. Lett.* **114**, 251603 (2015).
4. V. Khemani, R. Moessner, S. L. Sondhi, arXiv:1910.10745 [cond-mat.str-el] (2019).
5. D. V. Else, C. Monroe, C. Nayak, N. Y. Yao, *Annu. Rev. Condens. Matter Phys.* **11**, 467–499 (2020).

6. Z. Gong, R. Hamazaki, M. Ueda, *Phys. Rev. Lett.* **120**, 040404 (2018).
7. N. Y. Yao, C. Nayak, L. Balents, M. P. Zaletel, *Nat. Phys.* **16**, 438–447 (2020).
8. H. Keßler *et al*., *Phys. Rev. Lett.* **127**, 043602 (2021).
9. D. V. Else, B. Bauer, C. Nayak, *Phys. Rev. Lett.* **117**, 090402 (2016).
10. V. Khemani, A. Lazarides, R. Moessner, S. L. Sondhi, *Phys. Rev. Lett.* **116**, 250401 (2016).
11. N. Y. Yao, A. C. Potter, I.-D. Potirniche, A. Vishwanath, *Phys. Rev. Lett.* **118**, 030401 (2017).
12. J. Zhang *et al*., *Nature* **543**, 217–220 (2017).
13. A. Kyprianidis *et al*., *Science* **372**, 1192–1196 (2021).
14. S. Choi *et al*., *Nature* **543**, 221–225 (2017).
15. J. O'Sullivan *et al*., *New J. Phys.* **22**, 085001 (2020).
16. J. Rovny, R. L. Blum, S. E. Barrett, *Phys. Rev. Lett.* **120**, 180603 (2018).
17. S. Pal, N. Nishad, T. S. Mahesh, G. J. Sreejith, *Phys. Rev. Lett.* **120**, 180602 (2018).
18. J. Smits, L. Liao, H. T. C. Stoof, P. van der Straten, *Phys. Rev. Lett.* **121**, 185301 (2018).
19. S. Autti, V. B. Eltsov, G. E. Volovik, *Phys. Rev. Lett.* **120**, 215301 (2018).
20. P. Frey, S. Rachel, arXiv:2105.06632v1 [quant-ph] (2021).
21. D. V. Else, B. Bauer, C. Nayak, *Phys. Rev. X* **7**, 011026 (2017).
22. F. Machado, D. V. Else, G. D. Kahanamoku-Meyer, C. Nayak, N. Y. Yao, *Phys. Rev. X* **10**, 011043 (2020).
23. P. Peng, C. Yin, X. Huang, C. Ramanathan, P. Cappellaro, *Nat. Phys.* **17**, 444–447 (2021).
24. D. A. Abanin, E. Altman, I. Bloch, M. Serbyn, *Rev. Mod. Phys.* **91**, 021001 (2019).
25. L. D'Alessio, M. Rigol, *Phys. Rev. X* **4**, 041048 (2014).
26. M. Ippoliti, K. Kechedzhi, R. Moessner, S. Sondhi, V. Khemani, *PRX Quantum* **2**, 030346 (2021).
27. See supplementary materials.
28. C. E. Bradley *et al*., *Phys. Rev. X* **9**, 031045 (2019).
29. M. H. Abobeih *et al*., *Nature* **576**, 411–415 (2019).
30. We note that avalanche instabilities might destabilize MBL in power-law interacting systems, although such effects are outside of current experimental and numerical capabilities (*33*).
31. N. Y. Yao *et al*., *Phys. Rev. Lett.* **113**, 243002 (2014).
32. A. L. Burin, *Phys. Rev. B* **91**, 094202 (2015).
33. W. De Roeck, F. Huveneers, *Phys. Rev. B* **95**, 155129 (2017).
34. I. Schwartz *et al*., *Sci. Adv.* **4**, eaat8978 (2018).
35. A. Lazarides, S. Roy, F. Piazza, R. Moessner, *Phys. Rev. Res.* **2**, 022002 (2020).
36. L. M. K. Vandersypen, I. L. Chuang, *Rev. Mod. Phys.* **76**, 1037–1069 (2005).
37. J. Choi *et al*., *Phys. Rev. X* **10**, 031002 (2020).
38. J. Cai, A. Retzker, F. Jelezko, M. B. Plenio, *Nat. Phys.* **9**, 168–173 (2013).
39. I. Lovchinsky *et al*., *Science* **355**, 503–507 (2017).
40. F. Dolde *et al*., *Nat. Phys.* **9**, 139–143 (2013).
41. M. Pompili *et al*., *Science* **372**, 259–264 (2021).
42. X. Mi *et al*., arXiv:2107.13571 [quant-ph] (2021).
43. J. Randall, C. E. Bradley, F. V. van der Gronden, A. Galicia, M. H. Abobeih, M. Markham, D. J. Twitchen, F. Machado, N. Y. Yao, T. H. Taminiau, Data and plotting code for 'Many-body-localized discrete time crystal with a programmable spin-based quantum simulator,' Zenodo (2021). https://doi.org/10.5281/zenodo.5636045.

ACKNOWLEDGMENTS

We thank W. Hahn and V. V. Dobrovitski for valuable discussions and A. Breitweiser for experimental assistance. **Funding:** This work was supported by the Netherlands Organisation for Scientific Research (NWO/OCW) through a Vidi grant and as part of the Frontiers of Nanoscience (NanoFront) program and the Quantum Software Consortium program (Project no. 024.003.037/3368). This project has received funding from the European Research Council (ERC) under the European Union's Horizon 2020 research and innovation program (grant agreement no. 852410). This project (QIA) has received funding from the European Union's Horizon 2020 research and innovation program under grant agreement no. 820445. F.M. acknowledges support from the U.S. Department of Energy, Office of Science, Office of Basic Energy Sciences, Materials Sciences and Engineering Division and the Division of Chemical Sciences, Geosciences and Biosciences at LBNL under Contract no. DE-AC02-05-CH11231. N.Y.Y. acknowledges support from the DARPA DRINQS program (D18AC00033), the Army Research Office (grant no. W911NF2110262), the David and Lucile Packard foundation, and the W. M. Keck foundation. **Author contributions:** J.R., C.E.B., F.V.vdG., A.G., and T.H.T. devised and performed the experiments, developed theoretical calculations, and performed numerical simulations. J.R., C.E.B., F.V.vdG., A.G., F.M., N.Y.Y., and T.H.T. analyzed the data. J.R., C.E.B., M.H.A., and T.H.T. prepared the experimental apparatus. M.M. and D.J.T. grew the diamond sample. J.R., C.E.B., F.M., N.Y.Y., and T.H.T. wrote the manuscript with input from all authors. T.H.T. supervised the project. **Competing interests:** The authors declare no competing interests. **Data and materials availability:** The underlying data and software code for generating the plots presented in the main text and supplementary materials are available at Zenodo (*43*).

SUPPLEMENTARY MATERIALS

science.org/doi/10.1126/science.abk0603
Materials and Methods
Figs. S1 to S9
Tables S1 to S6
References (*44*–*58*)

25 June 2021; accepted 21 October 2021
Published online 4 November 2021
10.1126/science.abk0603

Science

Many-body–localized discrete time crystal with a programmable spin-based quantum simulator

J. RandallC. E. BradleyF. V. van der GrondenA. GaliciaM. H. AbobeihM. MarkhamD. J. TwitchenF. MachadoN. Y. YaoT. H. Taminiau

Science, 374 (6574), • DOI: 10.1126/science.abk0603

Establishing order, time after time
The formation of discrete time crystals, a novel phase of matter, has been proposed for some many-body quantum systems under periodic driving conditions. Randall *et al*. used an array of nuclear spins surrounding a nitrogen vacancy center in diamond as their many-body quantum system. Subjecting the system to a series of periodic driving pulses, they observed ordering of the spins occurring at twice the driving frequency, a signature that they claim establishes the formation of a discrete time crystal. Such dynamic control is expected to be useful for manipulating quantum systems and implementing quantum information protocols. —ISO